

APnP: A Less-constrained PnP Solver for Pose Estimation with Unknown Anisotropic Scaling or Focal Lengths

Jiaxin Wei^{*†}, Stefan Leutenegger^{*}, Laurent Kneip[†]

Abstract

Perspective- n -Point (PnP) stands as a fundamental algorithm for pose estimation in various applications. In this paper, we present a new approach to the PnP problem with relaxed constraints, eliminating the need for precise 3D coordinates or complete calibration data. We refer to it as APnP due to its ability to handle unknown anisotropic scaling factors of 3D coordinates or alternatively two distinct focal lengths in addition to the conventional rigid transformation. Through algebraic manipulations and a novel parametrization, both cases are brought into similar forms that distinguish themselves primarily by the order of a rotation and an anisotropic scaling operation. APnP then boils down to one unique polynomial problem, which is solved by the Gröbner basis approach. Experimental results on both simulated and real datasets demonstrate the effectiveness of APnP as a more flexible and practical solution to camera pose estimation. Code: <https://github.com/goldoak/APnP>.

1. Introduction

Camera pose estimation is an active area of research in both computer vision and robotics communities as it is indispensable in many practical applications such as visual localization, 3D reconstruction, and object tracking. The Perspective- n -Point problem is one of the most well-known techniques in this field, utilizing 2D image measurements and corresponding 3D landmarks in the environment to infer the camera pose. Many variants have been introduced over the years to continuously improve accuracy, efficiency, and robustness [23, 28, 31].

Traditional PnP solvers require 2D-3D correspondences and full intrinsic parameters for accurate pose estimation. Therefore, an exact 3D model must be available beforehand, which may impose significant limitations on the solver’s applicability, especially in scenarios where obtaining an exact

3D model is challenging [37]. Moreover, accurate calibration can be very time-consuming in practice. For example, Zhang’s calibration method [45] can only provide satisfactory intrinsic parameters when enough flat calibration patterns have been observed from different poses, resulting in increased data collection efforts. The direct linear transformation (DLT) algorithm [22] can recover all the unknown intrinsic parameters from only 6 points, but it often overfits noisy data.

To relax the strict assumptions of traditional methods, we propose a novel and less-constrained solver, APnP (Anisotropic PnP), allowing for more flexibility in estimating camera poses. Specifically, it can estimate the camera pose while accommodating two important cases (see Fig. 1):

1. **Anisotropic scaling of 3D coordinates:** The exact 3D model of an object may not be available in some practical scenarios (e.g. CAD model retrieval), but only a 3D shape prior is given up to unknown aspect ratios. APnP addresses this by simultaneously estimating the scaling factors along different axes such that the 3D shape prior can be aligned to the observed object in the 2D image after non-uniform stretching or compressing.
2. **Partial calibration with unknown focal lengths:** Given the exact 3D model, our APnP solver is able to work with limited intrinsic parameters, i.e. only the principal point is required, while the two focal lengths can be determined along with the camera pose. This is particularly useful for cameras with rectangular pixels (i.e. the pixel sizes along the width and height dimensions are different).

In the following section, we will demonstrate that with just a few manipulations, the equations for the above two problems can be brought into a very similar form. The key distinction between the two problems lies in the order of an anisotropic scaling operation and a 3D rotation. Despite this difference, the resulting polynomial systems of equations for both problems share an identical algebraic form.

In the experimental setup, we integrate the APnP solver into a RANSAC loop to effectively handle outlier correspondences and mitigate the effects of noise in the data. We also employ non-linear refinement techniques and optimize over unknown variables (i.e. rotation, translation,

^{*}Smart Robotics Lab, Department of Informatics, Technical University of Munich

[†]Mobile Perception Lab, School of Information Science and Technology, ShanghaiTech University

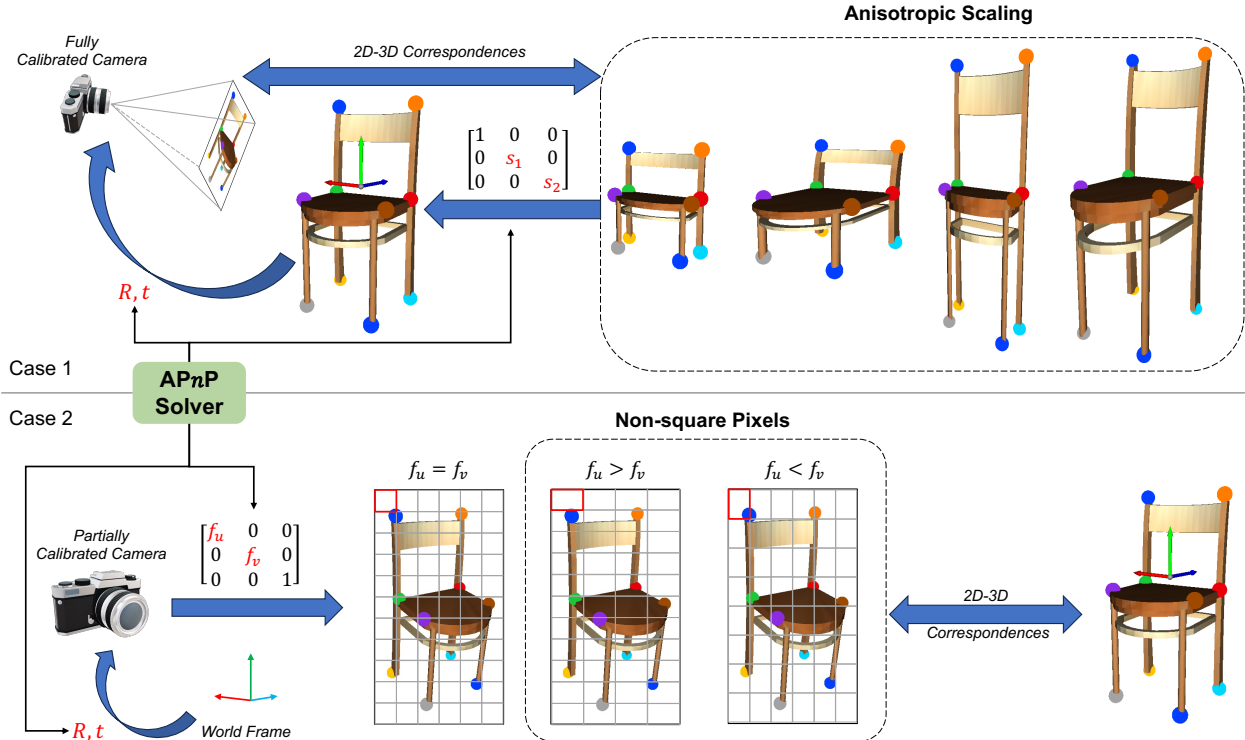


Figure 1. Illustration of the two practical cases in camera pose estimation which can be well handled by our proposed APnP solver. Specifically, it can simultaneously estimate anisotropic scaling factors or focal lengths in addition to the camera pose.

and scaling factors/focal lengths) to further enhance its performance. Evaluations on simulation data are conducted first to analyze the impact of different hyper-parameters involved in APnP. Extensive experiments on real datasets then demonstrate the clear superiority of RANSAC-APnP over the traditional PnP and 6-point DLT in cases where precise 2D-3D correspondences or complete calibration parameters are unavailable. Finally, to establish its practical applicability, we design a challenging experiment, leveraging only sparse keypoints to perform camera pose estimation with unknown anisotropic scaling or focal lengths. In summary, we make the following contributions:

1. We relax the constraints imposed by traditional PnP solvers and propose a novel APnP algorithm that can handle unknown anisotropic scaling or focal lengths while estimating the camera pose, providing a more flexible solution to this task.
2. Through algebraic manipulations, the APnP solver establishes a highly similar form for the two cases, differing only in the order of scaling and rotation operations. A new Gröbner basis solver is introduced to solve the resulting polynomial problem. We further introduce a secondary parametrization to reduce incidence relations from cubic to quadratic order.
3. Comprehensive experiments on both simulation and

real data prove the robustness and effectiveness of our RANSAC-APnP, showcasing its valuable advancement in the field of camera pose estimation.

2. Related Work

Camera pose estimation is first introduced within the photogrammetry community [13, 19, 35]. These early solutions including the first minimal solvers developed within the computer vision community [15, 17, 25, 33] are well reviewed in the work of Haralick et al. [21]. De Menthon and Davis [9] further propose exact and approximate solutions to the so-called Perspective-three-point (P3P) problem, while Gao et al. [16] present the first complete solution classification, analyzing the number of solutions as a function of both algebraic and geometric conditioning. Kneip et al. [27] contribute the first solution to the P3P problem that directly solves the camera pose parameters rather than the traditional formulation in terms of unknown depths along rays. The P3P problem remains one of the most fundamental geometric computer vision problems till modern times, as novel formulations that improve on execution speed, numerical robustness, or explainability of the solution number keep being discovered [4, 12, 26, 36, 38].

The P3P problem is a special case of the PnP problem. The first solution for PnP is the popular DLT algorithm in-

roduced by Sutherland in 1963 [42]. Improved solutions taking into account known camera calibration parameters are proposed later by Dhome et al. [11], De Menthon and Davis [10], and Horaud et al. [24]. The linear solutions to the problem are further investigated by Quan and Lan [39] and Ameller et al. [2], Fiore [14], and Ansar and Daniilidis [3], while Schweighofer and Pinz [40] solve the PnP problem based on a geometric error criterion. Notably, Lepetit et al. [31] propose another linear complexity solution to the PnP problem which is still considered as state-of-the-art when efficiency is the major concern. Another breed of solvers is later introduced by Hesch and Roumeliotis [23], Zheng et al. [46], and Kneip et al. [28], to which our APnP also belong. These solvers have linear complexity and find the global minimum of the sum of squared object space errors in closed form.

Of further importance to the work conducted here are camera pose estimation algorithms that address the partially calibrated case. Abidi and Chandra [1] solve the problem of camera pose and unknown focal length for planar point distributions while the first solution for non-planar scenes is introduced by Triggs [43]. Later, Bujnak proposes the first minimal solution that works in both planar and non-planar scenarios [6]. It is worth noting that those previous works only consider an unknown effective focal length, assuming the camera has square pixels. Guo [20] proposes to estimate a focal length and an aspect ratio based on the P4P problem. Larsson et al. [30] consider the case where an aspect ratio as well as the principal point and focal length are all unknown. To solve this problem, they construct a minimal solver using 5-point correspondences. We also discuss the partial calibration problem in our case 2 but with a slightly different parameterization of the intrinsic matrix, i.e. we assume only the two anisotropic focal lengths are unknown instead of using an aspect ratio to model the relation between the focal lengths along the horizontal and vertical directions of the image plane. This parameterization is to ensure consistency with our case 1, where we take into account two unknown anisotropic scaling of the reference model along the y and z -axis. This problem is rather new and has thus not been explored in current literature.

3. Theory

We begin with a clear problem formulation and introduce all relevant notations. From there, we proceed to derive the reprojection error and present the closed-form solver. Finally, we summarize the method and highlight some important implementation details.

3.1. Problem Formulation

As previously mentioned in the introduction, this work addresses two novel generalizations of the PnP problem applicable in the case where the observed 3D point cloud is

affected by unknown anisotropic scaling or the case where there are two unknown focal lengths in addition to the unknown camera pose. In the following, we will derive the algebraic formulation of these two cases:

Case 1 We have a fully calibrated camera \mathcal{C} and a 3D shape prior with unknown aspect ratios. We assume that the coordinates of the object along the x -axis are known without ambiguity, while the coordinates along the y and z -axis are affected by two independent scale factors s_1 and s_2 , respectively. Hence, we can obtain the projection function which transforms 3D world points \mathbf{x} into the normalized image plane:

$$\lambda \mathbf{u}' = \mathbf{R} \begin{bmatrix} 1 & 0 & 0 \\ 0 & s_1 & 0 \\ 0 & 0 & s_2 \end{bmatrix} \mathbf{x} + \mathbf{t}. \quad (1)$$

where λ denotes the depth along the principal axis and \mathbf{u}' is the normalized image coordinate with the third coordinate always being 1. Note that \mathbf{R} represents the rotation matrix from the world to the camera frame, and \mathbf{t} represents the position of the world origin seen from the camera frame.

Case 2 The 3D object is known absolutely but we have a partially calibrated camera \mathcal{C}' of which all parameters apart from focal lengths are given. Let f_u and f_v be the focal lengths along the horizontal and vertical directions of the image plane, respectively. We can obtain

$$\lambda \mathbf{u}'' = \begin{bmatrix} f_u & 0 & 0 \\ 0 & f_v & 0 \\ 0 & 0 & 1 \end{bmatrix} (\mathbf{R}\mathbf{x} + \mathbf{t}), \quad (2)$$

where \mathbf{u}'' is the centered and undistorted image point measured in pixels. By substituting (2) with

$$\lambda' = \frac{\lambda}{f_u}, s'_1 = \frac{f_v}{f_u}, s'_2 = \frac{1}{f_u}, \mathbf{t}' = \begin{bmatrix} 1 & 0 & 0 \\ 0 & s'_1 & 0 \\ 0 & 0 & s'_2 \end{bmatrix} \mathbf{t},$$

we can reduce (2) to a similar form as (1) in case 1

$$\lambda' \mathbf{u}'' = \begin{bmatrix} 1 & 0 & 0 \\ 0 & s'_1 & 0 \\ 0 & 0 & s'_2 \end{bmatrix} \mathbf{R}\mathbf{x} + \mathbf{t}'. \quad (3)$$

In summary, the two cases of unknown aspect ratios and unknown focal lengths are essentially similar problems, except for the order of the rotation matrix and the anisotropic scaling matrix. As demonstrated in the following sections, these two problems can be effectively reformulated into the same polynomial problem, requiring only one solver to address both.

3.2. Derivation of Reprojection Error

Inspired by the *UPnP* algorithm [28], we begin with (16) from case 1 to derive our reprojection error. Here we denote $\mathbf{Q} = \mathbf{R} \text{diag}(1, s_1, s_2)$ for mathematical convenience. Therefore, given n 2D-3D correspondences, we can establish an equation system

$$\begin{bmatrix} \mathbf{u}'_1 & & & -\mathbf{I} \\ & \ddots & & \vdots \\ & & \mathbf{u}'_n & -\mathbf{I} \end{bmatrix} \begin{bmatrix} \lambda_1 \\ \vdots \\ \lambda_n \\ \mathbf{t} \end{bmatrix} = \begin{bmatrix} \mathbf{Q} & & \\ & \ddots & \\ & & \mathbf{Q} \end{bmatrix} \begin{bmatrix} \mathbf{x}_1 \\ \vdots \\ \mathbf{x}_n \end{bmatrix}. \quad (4)$$

To simplify the mathematical expression and prepare for applying the Schur complement, we transform the equation into the following form:

$$\begin{bmatrix} \mathbf{u}'_1{}^T \mathbf{u}'_1 & & & -\mathbf{u}'_1{}^T \\ & \ddots & & \vdots \\ & & \mathbf{u}'_n{}^T \mathbf{u}'_n & -\mathbf{u}'_n{}^T \\ -\mathbf{u}'_1 & \cdots & -\mathbf{u}'_n & n\mathbf{I} \end{bmatrix} \begin{bmatrix} \lambda_1 \\ \vdots \\ \lambda_n \\ \mathbf{t} \end{bmatrix} = \begin{bmatrix} \mathbf{u}'_1{}^T \mathbf{Q} \mathbf{x}_1 \\ \vdots \\ \mathbf{u}'_n{}^T \mathbf{Q} \mathbf{x}_n \\ -\sum_i (\mathbf{Q} \mathbf{x}_i) \end{bmatrix}. \quad (5)$$

Please refer to the supplementary material for a detailed derivation of the Schur complement. In brief, we can obtain

$$\mathbf{t} = \mathbf{H}^{-1} \left\{ \sum_i \left(\frac{\mathbf{u}'_i \mathbf{u}'_i{}^T}{\mathbf{u}'_i{}^T \mathbf{u}'_i} - \mathbf{I} \right) \mathbf{Q} \mathbf{x}_i \right\}, \quad (6)$$

where

$$\mathbf{H} = \left\{ \sum_i \left(\mathbf{I} - \frac{\mathbf{u}'_i \mathbf{u}'_i{}^T}{\mathbf{u}'_i{}^T \mathbf{u}'_i} \right) \right\}.$$

and

$$\lambda_i = \frac{\mathbf{u}'_i{}^T}{\mathbf{u}'_i{}^T \mathbf{u}'_i} \left(\mathbf{Q} \mathbf{x}_i + \mathbf{H}^{-1} \left\{ \sum_i \mu(\mathbf{u}'_i) \mathbf{Q} \mathbf{x}_i \right\} \right), \quad (7)$$

with

$$\mu(\mathbf{u}'_i) = \frac{\mathbf{u}'_i \mathbf{u}'_i{}^T}{\mathbf{u}'_i{}^T \mathbf{u}'_i} - \mathbf{I}.$$

Next, we reformulate $\mathbf{Q} \mathbf{x}_i$ into $\Phi(\mathbf{x}_i) \mathbf{m}$ where $\Phi(\mathbf{x}_i) \in \mathbb{R}^{3 \times m}$, $\mathbf{m} \in \mathbb{R}^{m \times 1}$, such that \mathbf{m} is a vector composed of monomials of unknowns. The specific form of $\Phi(\mathbf{x}_i)$ and \mathbf{m} depends on the chosen parameterization, which will be discussed in Sec. 3.3.

By applying these reformulations, back-substituting (21) and (22) in (17), and taking the difference between the left and right-hand sides, we finally obtain the following compact expression for the reprojection error:

$$\epsilon_i = \mu(\mathbf{u}'_i) \left(\Phi(\mathbf{x}_i) + \mathbf{H}^{-1} \left\{ \sum_i \mu(\mathbf{u}'_i) \Phi(\mathbf{x}_i) \right\} \right) \mathbf{m},$$

which can be simply denoted as

$$\epsilon_i = \mathcal{A}_i \mathbf{m} \quad (8)$$

There are two important points to note:

- By adjusting the definition of \mathbf{Q} , the derivations and the final form are analogous if we start from (3). The primary difference lies in the internal form of $\Phi(\mathbf{x}_i)$.
- The derivations have been conducted for an arbitrary number of correspondences n . However, the minimum number of points required is 4 as the number of degrees of freedom is 8 (6 for Euclidean pose and 2 for scales).

3.3. Parametrization

Let us start with case 1, the problem of anisotropic scaling, where $\mathbf{Q} = \mathbf{R} \text{diag}(1, s_1, s_2)$. One straightforward approach for choosing the parametrization could involve using a quaternion-based parametrization for the rotation matrix along with the scale variables s_1 and s_2 . However, this approach would lead to a complex problem with six unknowns and result in polynomial constraints of order 5 after forming the sum of squared errors and first-order optimality conditions. We, therefore, propose an alternative parametrization.

Matrix \mathbf{Q} can be simply interpreted as having three orthogonal columns with arbitrary relative norms. We choose $[a \ b \ c]^T$ as the first column and make sure its norm is one ($a^2 + b^2 + c^2 = 1$). Then, $[d \ e \ f]^T$ becomes the second basis vector, and we ensure orthogonality by adding an extra constraint, i.e. $[a \ b \ c][d \ e \ f]^T = 0$. The third column is formed by the cross-product of the first and second columns, automatically fulfilling orthogonality. Note that the norm of the third column can be controlled by the norm of $[d \ e \ f]^T$. To maintain the independence of the norm of the second column, it is multiplied by an additional scale factor. Finally, we obtain

$$\mathbf{Q} = \begin{bmatrix} [a \\ b \\ c] & s [d \\ e \\ f] & [a \\ b \\ c] \times [d \\ e \\ f] \end{bmatrix}. \quad (9)$$

Using this formulation will result in seven unknowns (a, b, c, d, e, f , and s) but a quadratic equation, which leads to third-order polynomials after summing the squared errors and taking first-order derivatives. The definition of the monomial vector is then given by

$$\mathbf{m} = [a \ b \ c \ sd \ se \ sf \ bf \ ce \ cd \ af \ ae \ bd]^T. \quad (10)$$

Meanwhile, with $\mathbf{x}_i = [x_1 \ x_2 \ x_3]^T$, we can get

$$\Phi(\mathbf{x}_i) = \quad (11)$$

$$\begin{bmatrix} x_1 & 0 & 0 & x_2 & 0 & 0 & x_3 & -x_3 & 0 & 0 & 0 & 0 \\ 0 & x_1 & 0 & 0 & x_2 & 0 & 0 & 0 & x_3 & -x_3 & 0 & 0 \\ 0 & 0 & x_1 & 0 & 0 & x_2 & 0 & 0 & 0 & 0 & x_3 & -x_3 \end{bmatrix}.$$

As for the case of a partially calibrated camera, $\mathbf{Q}' = \text{diag}(1, s'_1, s'_2)\mathbf{R}$, the difference is given by the fact that now we have three arbitrarily scaled, orthogonal rows, i.e.

$$\mathbf{Q}' = \mathbf{Q}^T = \begin{bmatrix} a \\ b \\ c \end{bmatrix} \quad s \begin{bmatrix} d \\ e \\ f \end{bmatrix} \quad \begin{bmatrix} a \\ b \\ c \end{bmatrix} \times \begin{bmatrix} d \\ e \\ f \end{bmatrix} \quad (12)$$

As a result, the monomial vector \mathbf{m} can be left unchanged, whereas $\Phi(\mathbf{x}_i)$ needs to be redefined as:

$$\begin{bmatrix} x_1 & x_2 & x_3 & 0 & 0 & 0 & 0 & 0 & 0 & 0 & 0 & 0 \\ 0 & 0 & 0 & x_1 & x_2 & x_3 & 0 & 0 & 0 & 0 & 0 & 0 \\ 0 & 0 & 0 & 0 & 0 & 0 & x_1 & -x_1 & x_2 & -x_2 & x_3 & -x_3 \end{bmatrix}.$$

3.4. Closed Form Solution

Our objective function is then given as a minimization of the sum of reprojection errors

$$\underset{a,b,c,d,e,f,s}{\text{argmin}} \sum_i \|\epsilon_i\|_2^2 \text{ s.t. } \begin{cases} a^2 + b^2 + c^2 = 1 \\ ad + be + cf = 0 \end{cases} \quad (13)$$

The energy to be minimized can be reformulated as

$$\sum_i \|\epsilon_i\|_2^2 = \sum_i \epsilon_i^T \epsilon_i = \mathbf{m}^T \left[\sum_i \mathcal{A}_i^T \mathcal{A}_i \right] \mathbf{m}, \quad (14)$$

Consequently, the minimum of the energy is finally retrieved in closed form by taking the first-order optimality conditions and solving the resulting cubic polynomial equation system

$$\begin{cases} 2\mathbf{m}^T \left[\sum_i \mathcal{A}_i^T \mathcal{A}_i \right] \frac{\partial \mathbf{m}}{\partial a} = 0 \\ 2\mathbf{m}^T \left[\sum_i \mathcal{A}_i^T \mathcal{A}_i \right] \frac{\partial \mathbf{m}}{\partial b} = 0 \\ 2\mathbf{m}^T \left[\sum_i \mathcal{A}_i^T \mathcal{A}_i \right] \frac{\partial \mathbf{m}}{\partial c} = 0 \\ 2\mathbf{m}^T \left[\sum_i \mathcal{A}_i^T \mathcal{A}_i \right] \frac{\partial \mathbf{m}}{\partial d} = 0 \\ 2\mathbf{m}^T \left[\sum_i \mathcal{A}_i^T \mathcal{A}_i \right] \frac{\partial \mathbf{m}}{\partial e} = 0 \\ 2\mathbf{m}^T \left[\sum_i \mathcal{A}_i^T \mathcal{A}_i \right] \frac{\partial \mathbf{m}}{\partial f} = 0 \\ 2\mathbf{m}^T \left[\sum_i \mathcal{A}_i^T \mathcal{A}_i \right] \frac{\partial \mathbf{m}}{\partial s} = 0 \\ a^2 + b^2 + c^2 = 1 \\ ad + be + cf = 0 \end{cases} \quad (15)$$

3.5. Solver Implementation

Solving the above system of polynomial equations is a complicated task that requires the application of algebraic geometry theory [8]. In this work, we develop a minimal solver based on the Gröbner basis method [5]. The solver is generated automatically using a C++ implementation of Kukulova et al.'s [29] automatic solver generation method, which relies on *Macaulay 2* [18]. The resulting elimination template is relatively large and has a size of 1531×1941 , and at most 16 solutions are obtained from the concluding Action matrix step.

4. Experiments

In this section, we analyze the performance of APnP on simulated data, compare it with traditional PnP and standard 6-point DLT [22] on real datasets, and demonstrate its practical applicability in a challenging experiment using only sparse keypoints to infer camera pose and unknown anisotropic scaling factors or focal lengths.

Comparisons We establish three methods for comparison, i.e. PnP, 6-point DLT (6p-DLT), and APnP. Each of these solvers is equipped with a RANSAC loop to handle potential noise and outlier correspondences in the input effectively. It is also worth noting that we leverage a minimal APnP solver here for the sake of efficiency. As known, the PnP method requires complete calibration parameters and precise 2D-3D correspondences to function properly. Hence, we only utilize it as a rough baseline in case 1. To improve the performance of RANSAC-APnP, we introduce a non-linear refinement step, further optimizing over desired unknown variables, including rotation, translation, and anisotropic scaling factors/focal lengths. For a fair comparison, we also perform the same non-linear refinement for RANSAC-6p-DLT.

Metrics We employ a set of metrics to evaluate the performance of our proposed method. Specifically, we report four key metrics:

- Rotation error: $R_{err} = \arccos((\text{trace}(\mathbf{R}_{gt}^T \mathbf{R}) - 1)/2)$
- Translation error: $t_{err} = \|\mathbf{t} - \mathbf{t}_{gt}\|_2$
- Anisotropic s_1/s_2 error: $s_{err} = |s - s_{gt}|/s_{gt}$
- Anisotropic f_u/f_v error: $f_{err} = |f - f_{gt}|/f_{gt}$

4.1. Simulation Data

In the following section, we focus on testing anisotropic scaling factors, as the two cases mentioned above are equivalent in essence. Therefore, the conclusions drawn from this analysis can also be generalized to the other case.

Data preparation We considered a virtual camera with an image resolution of 640×480 , a principal point at $(u_c, v_c) = (320, 240)$, and a focal length of $f_u = f_v = 150$. The 3D points were randomly sampled from the interval of $[-1, 1) \times [-1, 1) \times [-1, 1)$, and the 2D points were consequently computed using the defined intrinsic parameters and a random rigid transformation each time ensuring that all points lie in front of the camera. Note that we randomly selected different scaling factors within the range of $[0.5, 2.0]$ to respectively scale the coordinates along the y-axis and z-axis, resulting in a new set of 3D coordinates that forms the synthetic 2D-3D correspondences we actually used in our test. All simulations were independently run 2000 times to ensure data diversity and each time we

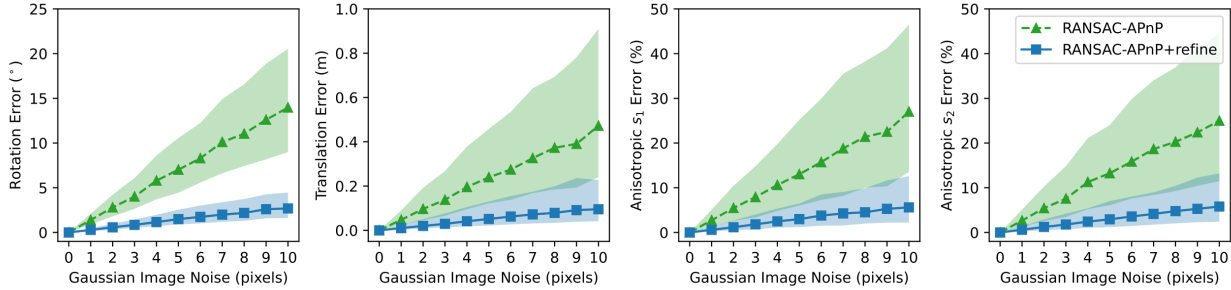


Figure 2. Statistical plot of different metrics with respect to Gaussian image noise. Lines with markers represent the median errors of different methods while the corresponding shaded area indicates IQR, the difference between the 75th and 25th percentiles of the data.

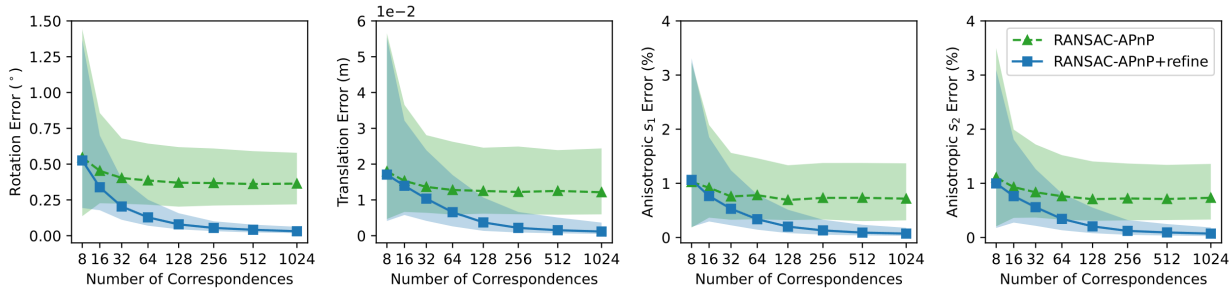


Figure 3. Statistical plot of different metrics with respect to the number of correspondences. Lines with markers represent the median errors of different methods while the corresponding shaded area indicates IQR, the difference between the 75th and 25th percentiles of the data.

generated 1024 correspondences as the default, unless otherwise specified.

Robustness to noise To test the robustness against noise, we add different amounts of Gaussian noise to 2D image points. The statistical results are shown in Fig. 2. As expected, the errors for all metrics increase with the noise levels. Meanwhile, the inclusion of non-linear optimization not only reduces the errors of RANSAC-APnP by a large margin but also enhances its stability. This can be observed from the interquartile range (IQR) represented by the shaded area in the graph. The data after non-linear optimization is more concentrated compared to the data before optimization, indicating improved stability.

Effect of the number of correspondences We further explore the impact of the total number of correspondences on our method by varying the number of correspondences used in each test. Additionally, to better visualize the results, we introduce Gaussian image noise with a standard deviation of 0.2. As shown in Fig. 3, the errors for all metrics decrease when the total number of correspondences increases, but the rate of decrease slowed down after reaching a certain threshold. Therefore, we suggest using as many cor-

respondences as possible without compromising efficiency. Notably, the method with non-linear refinement exhibits a more significant reduction in errors, and the data points become more concentrated, demonstrating consistent superiority over RANSAC-APnP.

4.2. Real Data

Datasets In this section, we conduct our experiments for both cases on two real datasets, NYU-RGBD [41] and MegaDepth [32]. Here we use the pre-processed data provided by [34]. Specifically, they generated 10000 2D-3D testing pairs based on the NYU-RGBD dataset, with each pair containing 1000 data points. The 3D transformations were manually generated in a certain way, and Gaussian image noise ($\sigma = 2$) was added to the 2D points. The MegaDepth dataset is more challenging as it collects images from the internet and exhibits diverse camera poses. [34] generated 10795 2D-3D testing pairs based on the MegaDepth dataset, with the number of data points in each pair varying from tens to thousands.

We manipulate the anisotropic scaling of 3D points or anisotropic focal lengths in the same way as for simulation data described in Sec. 4.1. Scaling factors are randomly drawn from $[0.5, 2.0]$ to either scale the coordinates along the y-axis and z-axis or scale the two focal lengths in the in-

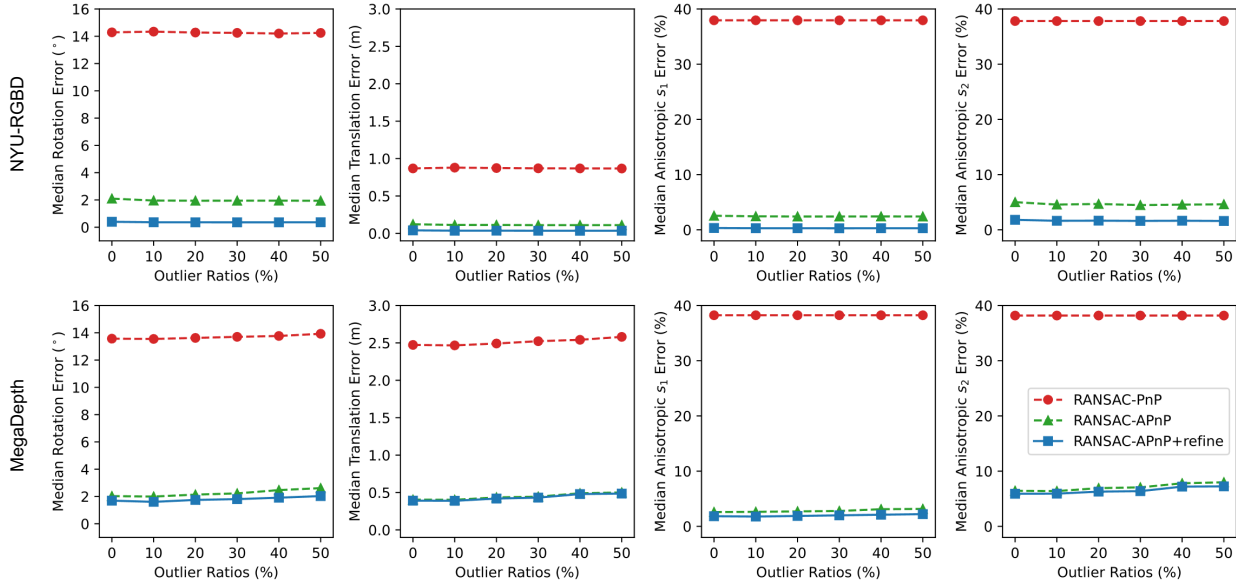


Figure 4. Case 1: APnP vs. PnP. Here shows different metrics with respect to outlier ratios on two real datasets.

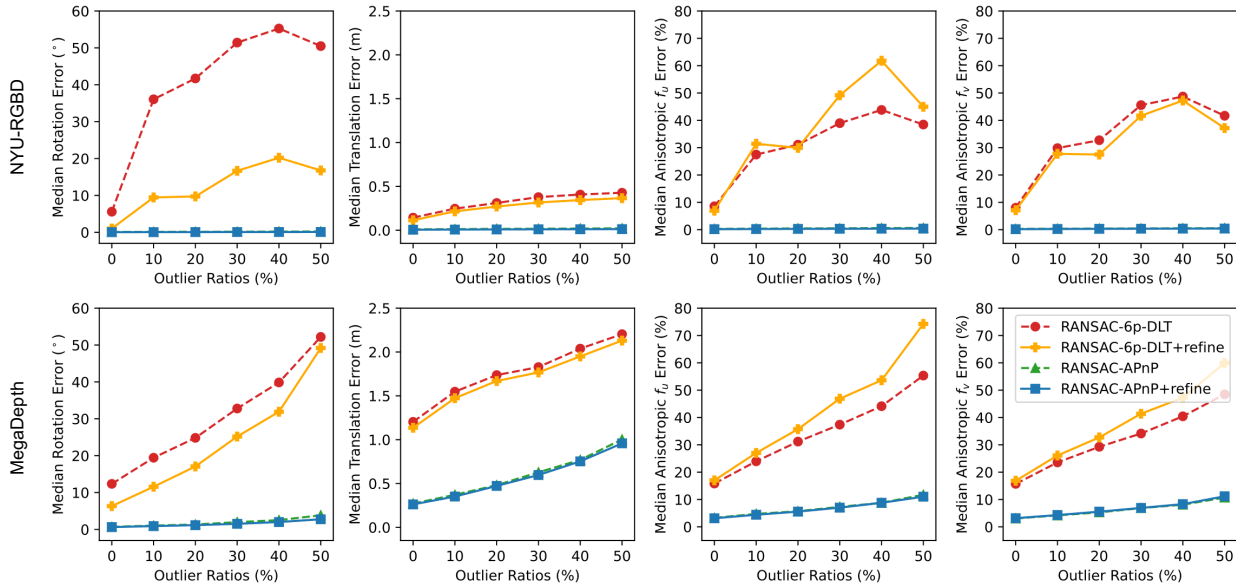


Figure 5. Case 2: APnP vs. 6p-DLT. Here shows different metrics with respect to outlier ratios on two real datasets.

trinsic matrix, generating updated 2D-3D pairs for our purpose. Note that in case 2 we have to adjust the 2D coordinates provided by the original datasets accordingly, therefore we manually add a small amount of image noise to the new set of 2D coordinates.

Case 1: anisotropic scaling For case 1, We evaluate three methods and present the results in Fig. 4. As we known, traditional PnP is incapable of handling additional anisotropic

scaling factors that exist in 3D coordinates, thereby resulting in high errors for all metrics. In contrast, our proposed APnP solver takes into account these unknown factors and successfully recovers the camera pose as well as the two scaling factors with significantly lower errors. With the help of the non-linear refinement step, it achieves better results, consistent with the findings from the simulation experiments.

Case 2: anisotropic focal length We conduct a similar experiment for case 2 but with the 6-point DLT as our baseline. While the DLT algorithm has the capability to estimate the full projection matrix, including both intrinsic and extrinsic parameters, it demonstrates susceptibility to the presence of noise and outliers in real data, even when employing a RANSAC loop and non-linear optimization techniques as depicted in Fig. 5. Besides, we can observe that not all metrics of 6-point DLT can be optimized via non-linear refinement. The rotation error of RANSAC-6p-DLT followed by a refinement decreases as the focal length error increases due to the interdependence among parameters in the projection matrix.

Given the broader error range associated with the 6-point DLT, it is hard to distinguish the performance difference between our proposed methods with or without refinement. We refer readers to the supplementary material for a detailed look at Fig. 5.

4.3. Sparse Keypoints Test

We further demonstrate the possibility of AP n P in a demanding scenario where only sparse keypoints are available for estimation. This situation frequently arises in object-related tasks, such as CAD model retrieval and alignment, where the keypoints may originate from manual annotation or keypoint detection.

Dataset KeypointNet [44] is a large-scale dataset extended from ShapeNet [7], containing numerous 3D models with manually annotated 3D keypoints. We selected 4 categories from KeypointNet, namely chair, bottle, car, and vessel. Each instance within the same category was rendered from a specific viewpoint to ensure the visibility of 3D keypoints. Finally, we obtain a subset consisting of 429 chairs, 255 bottles, 968 cars, and 421 vessels where each instance has at least 4 keypoints in rendered 2D images. The post-processing procedures for both case 1 and case 2 are identical to those described in Sec. 4.2.

Results Based on the insights from Fig. 3, we find that non-linear refinement does not significantly impact performance when dealing with a limited number of 2D-3D correspondences. Therefore, we leverage RANSAC-AP n P for the sparse keypoints test. The results for case 1 and case 2 are presented in Table 1 and 2, respectively. Remarkably, our proposed method consistently achieves low median errors for all metrics, even with an average of 6-9 keypoint pairs. To gain a better understanding of case 1, we show some qualitative results in Fig. 6. It can be seen that the objects in 2D images are tightly enclosed by the estimated bounding boxes (red), which indicates the high accuracy of our approach.

Category	Metrics				
	Avg. keypoints	Med. R err. (°)	Med. t err. (m)	Med. s_1 err. (%)	Med. s_2 err. (%)
chair	6	0.234	0.002	0.3	0.7
bottle	6	0.793	0.006	1.0	1.6
car	9	0.272	0.005	0.7	0.5
vessel	6	1.132	0.012	2.3	1.1

Table 1. Case 1. Median errors of RANSAC-AP n P on Keypoint-Net dataset.

Category	Metrics				
	Avg. keypoints	Med. R err. (°)	Med. t err. (m)	Med. f_u err. (%)	Med. f_v err. (%)
chair	6	0.121	0.010	1.0	1.0
bottle	6	1.528	0.112	10.2	11.0
car	9	0.523	0.036	3.4	2.8
vessel	6	1.888	0.083	6.6	6.0

Table 2. Case 2. Median errors of RANSAC-AP n P on Keypoint-Net dataset.

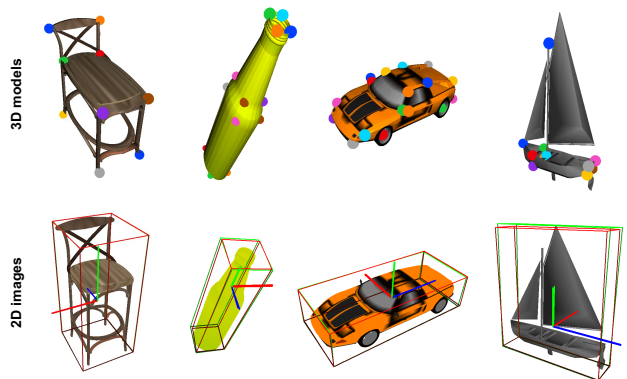


Figure 6. Qualitative results on KeypointNet dataset (case 1). The ground truth and predictions are denoted by green and red bounding boxes, respectively. The length of the axis also indicates the anisotropic scaling applied along that dimension.

5. Conclusion

In conclusion, we have introduced a novel AP n P solver that reduces the heavy reliance on precise 3D models or strict calibration conditions, which are typically required by traditional P n P solvers and camera calibration methods. This solver can estimate the camera pose, along with anisotropic scaling factors or focal lengths according to the application. Through mathematical derivations, we have revealed that these two seemingly different problems share a common algebraic structure and therefore can be solved by one polynomial solver. Extensive experiments on both simulation and real data have demonstrated the effectiveness of our RANSAC-AP n P, showing its potential to make camera pose estimation more flexible in practical settings. Our future work will delve into different parameterizations and solver generators to further improve efficiency and robustness of this new problem.

References

- [1] M.A. Abidi and T.D. Chandra. A new efficient and direct solution for pose estimation using quadrangular targets: algorithm and evaluation. *IEEE Transactions on Pattern Analysis and Machine Intelligence (PAMI)*, 17(5):534–538, 1995. 3
- [2] M.-A. Ameller, B. Triggs, and L. Quan. Camera pose revisited—new linear algorithms. In *In Archive ouverte HAL: Open science*, 2000. 3
- [3] A. Ansar and K. Daniilidis. Linear pose estimation from points or lines. *IEEE Transactions on Pattern Analysis and Machine Intelligence (PAMI)*, 25(5):578–589, 2003. 3
- [4] A. Banno. A p3p problem solver representing all parameters as a linear combination. *Image and Vision Computing (IVC)*, 70:55–62, 2018. 2
- [5] B. Buchberger. *Multidimensional Systems Theory - Progress, Directions and Open Problems in Multidimensional Systems*. Reidel Publishing Company, Dordrecht - Boston - Lancaster, 1985. 5
- [6] M. Bujnak, Z. Kukelova, and T. Pajdla. A general solution to the p4p problem for camera with unknown focal length. In *Proceedings of the IEEE Conference on Computer Vision and Pattern Recognition (CVPR)*, 2008. 3
- [7] Angel X Chang, Thomas Funkhouser, Leonidas Guibas, Pat Hanrahan, Qixing Huang, Zimo Li, Silvio Savarese, Manolis Savva, Shuran Song, Hao Su, et al. Shapenet: An information-rich 3d model repository. *arXiv preprint arXiv:1512.03012*, 2015. 8
- [8] David Cox, John Little, Donal O’Shea, and Moss Sweedler. Ideals, varieties, and algorithms. *American Mathematical Monthly*, 101(6):582–586, 1994. 5
- [9] D.F. De Menthon and L.S. Davis. Exact and approximate solutions of the perspective-three-point problem. *IEEE Transactions on Pattern Analysis and Machine Intelligence (PAMI)*, 14(11):1100–1105, 1992. 2
- [10] D.F. De Menthon and L.S. Davis. Model-based object pose in 25 lines of code. *International Journal of Computer Vision (IJCV)*, 15(1–2):123–141, 1995. 3
- [11] M. Dhome, M. Richetin, and J.T. Lapreste. Determination of the attitude of 3D objects from a single perspective view. *IEEE Transactions on Pattern Analysis and Machine Intelligence (PAMI)*, 11(12):1265–1278, 1989. 3
- [12] Y. Ding, J. Yang, V. Larsson, C. Olsson, and K. Åström. Revisiting the p3p problem. In *Proceedings of the IEEE Conference on Computer Vision and Pattern Recognition (CVPR)*, 2023. 2
- [13] S. Finsterwalder and W. Scheufele. *Das Rückwärtseinschneiden im Raum*. Verlag Herbert Wichmann, Berlin, Germany, 1937. 2
- [14] P.D. Fiore. Efficient linear solution of exterior orientation. *IEEE Transactions on Pattern Analysis and Machine Intelligence (PAMI)*, 23(2):140–148, 2001. 3
- [15] M.A. Fischler and R.C. Bolles. Random sample consensus: a paradigm for model fitting with applications to image analysis and automated cartography. *Communications of the ACM*, 24(6):381–395, 1981. 2
- [16] X.S. Gao, X.R. Hou, J. Tang, and H.F. Cheng. Complete solution classification for the perspective-three-point problem. *IEEE Transactions on Pattern Analysis and Machine Intelligence (PAMI)*, 25(8):930–943, 2003. 2
- [17] E.W. Grafarend, P. Lohse, and B. Schaffrin. Dreidimensionaler Rückwärtsschnitt, Teil 1: Die projektiven Gleichungen. *Zeitschrift für Vermessungswesen, Geodätisches Institut, Universität Stuttgart*, pages 1–37, 1989. 2
- [18] Daniel R. Grayson and Michael E. Stillman. Macaulay2, a software system for research in algebraic geometry. Available at <http://www.math.uiuc.edu/Macaulay2/>. 5
- [19] J.A. Grunert. Das pothenotische Problem in erweiterter Gestalt nebst über seine Anwendungen in Geodäsie. In *Grunerts Archiv für Mathematik und Physik*, 1841. 2
- [20] Yang Guo. A novel solution to the p4p problem for an uncalibrated camera. *Journal of mathematical imaging and vision*, 45:186–198, 2013. 3
- [21] R.M. Haralick, C. Lee, K. Ottenberg, and M. Nolle. Analysis and solutions of the three point perspective pose estimation problem. In *Proceedings of the IEEE Conference on Computer Vision and Pattern Recognition (CVPR)*, Maui, USA, 1991. 2
- [22] Richard Hartley and Andrew Zisserman. *Multiple view geometry in computer vision*. Cambridge university press, 2003. 1, 5
- [23] J.A. Hesch and S.I. Roumeliotis. A Direct Least-Squares (DLS) Method for PnP. In *Proceedings of the International Conference on Computer Vision (ICCV)*, 2011. 1, 3
- [24] R. Horaud, B. Conio, and O. Le Boulleux. An analytic solution for the perspective 4-point problem. *Computer Vision, Graphics, and Image Processing*, 47(1):33–44, 1989. 3
- [25] Y. Hung, P. Yeh, and D. Harwood. Passive ranging to known planar point sets. In *Proceedings of the IEEE International Conference on Robotics and Automation (ICRA)*, San Francisco, CA, USA, 1986. 2
- [26] T. Ke and S. I. Roumeliotis. An efficient algebraic solution to the perspective-three-point problem. In *Proceedings of the IEEE Conference on Computer Vision and Pattern Recognition (CVPR)*, 2017. 2
- [27] L. Kneip, D. Scaramuzza, and R. Siegwart. A novel parametrization of the perspective-three-point problem for a direct computation of absolute camera position and orientation. In *Proceedings of the IEEE Conference on Computer Vision and Pattern Recognition (CVPR)*, 2013. 2
- [28] Laurent Kneip, Hongdong Li, and Yongdook Seo. Upnp: An optimal o(n) solution to the absolute pose problem with universal applicability. In *Proceedings of the European Conference on Computer Vision (ECCV)*, pages 127–142. Springer, 2014. 1, 3, 4
- [29] Zuzana Kukelova, Martin Bujnak, and Tomas Pajdla. Automatic generator of minimal problem solvers. In *Proceedings of the European Conference on Computer Vision (ECCV)*, pages 302–315, 2008. 5
- [30] Viktor Larsson, Zuzana Kukelova, and Yinqiang Zheng. Camera pose estimation with unknown principal point. In *Proceedings of the IEEE Conference on Computer Vision and Pattern Recognition*, pages 2984–2992, 2018. 3
- [31] V. Lepetit, F. Moreno-Noguer, and P. Fua. EPnP: An accurate O(n) solution to the PnP problem. *International Journal of Computer Vision (IJCV)*, 81(2):578–589, 2009. 1, 3

- [32] Zhengqi Li and Noah Snavely. Megadepth: Learning single-view depth prediction from internet photos. In *Proceedings of the IEEE conference on computer vision and pattern recognition*, pages 2041–2050, 2018. 6, 11
- [33] S. Linnainmaa, D. Harwood, and L.S. Davis. Pose estimation of a three-dimensional object using triangle pairs. *IEEE Transactions on Pattern Analysis and Machine Intelligence (PAMI)*, 10(5):634–647, 1988. 2
- [34] Liu Liu, Dylan Campbell, Hongdong Li, Dingfu Zhou, Xibin Song, and Ruigang Yang. Learning 2d-3d correspondences to solve the blind perspective-n-point problem. *arXiv preprint arXiv:2003.06752*, 2020. 6
- [35] E.L. Merritt. Explicit three-point resection in space. *Photogrammetric Engineering*, 15(4):649–655, 1949. 2
- [36] Gaku Nakano. A simple direct solution to the perspective-three-point problem. In *Proceedings of the British Machine Vision Conference (BMVC)*, 2019. 2
- [37] Vojtech Panek, Zuzana Kukelova, and Torsten Sattler. Visual localization using imperfect 3d models from the internet. In *Proceedings of the IEEE/CVF Conference on Computer Vision and Pattern Recognition*, pages 13175–13186, 2023. 1
- [38] M. Persson and K. Nordberg. Lambda Twist: An Accurate Fast Robust Perspective Three Point (P3P) Solver. In *Proceedings of the European Conference on Computer Vision (ECCV)*, 2018. 2
- [39] L. Quan and Z. Lan. Linear n-point camera pose determination. *IEEE Transactions on Pattern Analysis and Machine Intelligence (PAMI)*, 21(8):774–780, 1999. 3
- [40] G. Schweighofer and A. Pinz. Robust pose estimation from a planar target. *IEEE Transactions on Pattern Analysis and Machine Intelligence (PAMI)*, 28(12):2024–2030, 2006. 3
- [41] Nathan Silberman, Derek Hoiem, Pushmeet Kohli, and Rob Fergus. Indoor segmentation and support inference from rgb-d images. In *Computer Vision–ECCV 2012: 12th European Conference on Computer Vision, Florence, Italy, October 7–13, 2012, Proceedings, Part V 12*, pages 746–760. Springer, 2012. 6, 11
- [42] I. Sutherland. Sketchpad: A man machine graphical communications system, 1963. Technical Report 296, MIT Lincoln Laboratories. 3
- [43] B. Triggs. Camera pose and calibration from 4 or 5 known 3D points. In *Proceedings of the International Conference on Computer Vision (ICCV)*, 1999. 3
- [44] Yang You, Yujing Lou, Chengkun Li, Zhoujun Cheng, Liangwei Li, Lizhuang Ma, Cewu Lu, and Weiming Wang. Keypointnet: A large-scale 3d keypoint dataset aggregated from numerous human annotations. In *Proceedings of the IEEE/CVF Conference on Computer Vision and Pattern Recognition*, pages 13647–13656, 2020. 8
- [45] Z. Zhang. A flexible new technique for camera calibration. *IEEE Transactions on Pattern Analysis and Machine Intelligence (PAMI)*, 22(11):1330–1334, 2000. 1
- [46] Y. Zheng, Y. Kuang, S. Sugimoto, K. Astrom, and M. Okutomi. Revisiting the PnP problem: A fast, general and optimal solution. In *Proceedings of the International Conference on Computer Vision (ICCV)*, 2013. 3

APnP: A Less-constrained PnP Solver for Pose Estimation with Unknown Anisotropic Scaling or Focal Lengths

Supplementary Material

6. Derivation Details of Schur Complement

In case 1, we assume that the coordinates of the object along the x -axis are known without ambiguity, while the coordinates along the y and z -axis are affected by two independent scale factors s_1 and s_2 , respectively. Hence, we can obtain the projection function which transforms 3D world points \mathbf{x} into the normalized image plane:

$$\lambda \mathbf{u}' = \mathbf{R} \begin{bmatrix} 1 & 0 & 0 \\ 0 & s_1 & 0 \\ 0 & 0 & s_2 \end{bmatrix} \mathbf{x} + \mathbf{t}. \quad (16)$$

where λ denotes the depth along the principal axis and \mathbf{u}' is the normalized image coordinate with the third coordinate always being 1. Note that \mathbf{R} represents the rotation matrix from the world to the camera frame, and \mathbf{t} represents the position of the world origin seen from the camera frame.

Here we denote $\mathbf{Q} = \mathbf{R} \text{diag}(1, s_1, s_2)$ for mathematical convenience. Therefore, given n 2D-3D correspondence, we can establish an equation system

$$\begin{bmatrix} \mathbf{u}'_1 & & & -\mathbf{I} \\ & \ddots & & \vdots \\ & & \mathbf{u}'_n & -\mathbf{I} \end{bmatrix} \begin{bmatrix} \lambda_1 \\ \vdots \\ \lambda_n \\ \mathbf{t} \end{bmatrix} = \begin{bmatrix} \mathbf{Q} & & \\ & \ddots & \\ & & \mathbf{Q} \end{bmatrix} \begin{bmatrix} \mathbf{x}_1 \\ \vdots \\ \mathbf{x}_n \end{bmatrix}. \quad (17)$$

To simplify the mathematical expression and prepare for applying the Schur complement, we transform the equation into the following form:

$$\begin{bmatrix} \mathbf{u}'_1{}^T \mathbf{u}'_1 & & & -\mathbf{u}'_1{}^T \\ & \ddots & & \vdots \\ & & \mathbf{u}'_n{}^T \mathbf{u}'_n & -\mathbf{u}'_n{}^T \\ -\mathbf{u}'_1 & \cdots & -\mathbf{u}'_n & n\mathbf{I} \end{bmatrix} \begin{bmatrix} \lambda_1 \\ \vdots \\ \lambda_n \\ \mathbf{t} \end{bmatrix} = \begin{bmatrix} \mathbf{u}'_1{}^T \mathbf{Q} \mathbf{x}_1 \\ \vdots \\ \mathbf{u}'_n{}^T \mathbf{Q} \mathbf{x}_n \\ -\sum_i (\mathbf{Q} \mathbf{x}_i) \end{bmatrix}. \quad (18)$$

By applying the Schur complement trick to (18), we arrive at the following result:

$$\begin{bmatrix} \lambda_1 \\ \vdots \\ \lambda_n \end{bmatrix} = \begin{bmatrix} \frac{\mathbf{u}'_1{}^T}{\mathbf{u}'_1{}^T \mathbf{u}'_1} (\mathbf{Q} \mathbf{x}_1 + \mathbf{t}) \\ \vdots \\ \frac{\mathbf{u}'_n{}^T}{\mathbf{u}'_n{}^T \mathbf{u}'_n} (\mathbf{Q} \mathbf{x}_n + \mathbf{t}) \end{bmatrix}, \quad (19)$$

and

$$\left(n\mathbf{I} - [\mathbf{u}'_1 \cdots \mathbf{u}'_n] \begin{bmatrix} \frac{1}{\mathbf{u}'_1{}^T \mathbf{u}'_1} & & \\ & \ddots & \\ & & \frac{1}{\mathbf{u}'_n{}^T \mathbf{u}'_n} \end{bmatrix} \begin{bmatrix} \mathbf{u}'_1{}^T \\ \vdots \\ \mathbf{u}'_n{}^T \end{bmatrix} \right) \mathbf{t} =$$

$$-\sum_i \mathbf{Q} \mathbf{x}_i + [\mathbf{u}'_1 \cdots \mathbf{u}'_n] \begin{bmatrix} \frac{1}{\mathbf{u}'_1{}^T \mathbf{u}'_1} & & \\ & \ddots & \\ & & \frac{1}{\mathbf{u}'_n{}^T \mathbf{u}'_n} \end{bmatrix} \begin{bmatrix} \mathbf{u}'_1{}^T \mathbf{Q} \mathbf{x}_1 \\ \vdots \\ \mathbf{u}'_n{}^T \mathbf{Q} \mathbf{x}_n \end{bmatrix} \\ \Leftrightarrow \left\{ \sum_i \left(\mathbf{I} - \frac{\mathbf{u}'_i \mathbf{u}'_i{}^T}{\mathbf{u}'_i{}^T \mathbf{u}'_i} \right) \right\} \mathbf{t} = \left\{ \sum_i \left(\frac{\mathbf{u}'_i \mathbf{u}'_i{}^T}{\mathbf{u}'_i{}^T \mathbf{u}'_i} - \mathbf{I} \right) \mathbf{Q} \mathbf{x}_i \right\} \quad (20)$$

From (20), we can obtain

$$\mathbf{t} = \mathbf{H}^{-1} \left\{ \sum_i \left(\frac{\mathbf{u}'_i \mathbf{u}'_i{}^T}{\mathbf{u}'_i{}^T \mathbf{u}'_i} - \mathbf{I} \right) \mathbf{Q} \mathbf{x}_i \right\}, \quad (21)$$

where

$$\mathbf{H} = \left\{ \sum_i \left(\mathbf{I} - \frac{\mathbf{u}'_i \mathbf{u}'_i{}^T}{\mathbf{u}'_i{}^T \mathbf{u}'_i} \right) \right\}.$$

Then, by performing back substitution into (19), we further get

$$\lambda_i = \frac{\mathbf{u}'_i{}^T}{\mathbf{u}'_i{}^T \mathbf{u}'_i} \left(\mathbf{Q} \mathbf{x}_i + \mathbf{H}^{-1} \left\{ \sum_i \mu(\mathbf{u}'_i) \mathbf{Q} \mathbf{x}_i \right\} \right), \quad (22)$$

with

$$\mu(\mathbf{u}'_i) = \frac{\mathbf{u}'_i \mathbf{u}'_i{}^T}{\mathbf{u}'_i{}^T \mathbf{u}'_i} - \mathbf{I}.$$

7. Supplementary Experiment Figure (Case 2)

We conduct an experiment for case 2 on two real datasets, NYU-RGBD [41] and MegaDepth [32]. Here we use 6-point DLT as our baseline and the results are shown in Fig. 7 (same as Fig. 5 in the main paper). Given the broader error range associated with the 6-point DLT, it is hard to distinguish the performance difference between our proposed methods with or without refinement in Fig. 7. Therefore, we add a supplementary figure (see Fig. 8) in which we omit the comparisons with 6-point DLT to better visualize the performance gap between our proposed methods.

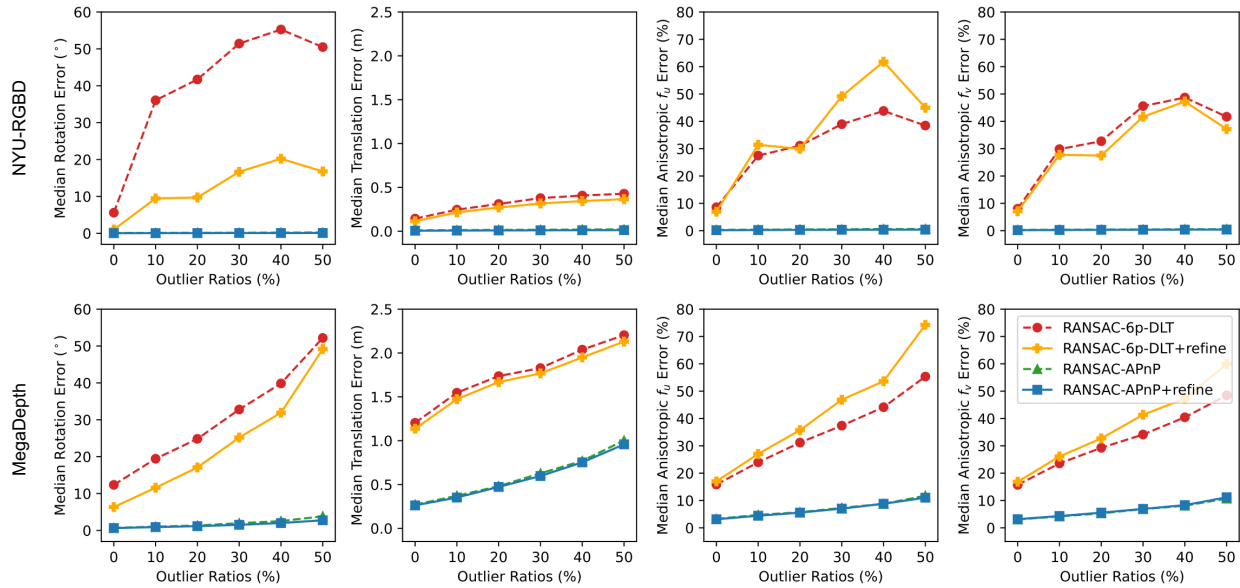


Figure 7. Case 2: APnP vs. 6p-DLT. Here shows different metrics with respect to outlier ratios on two real datasets.

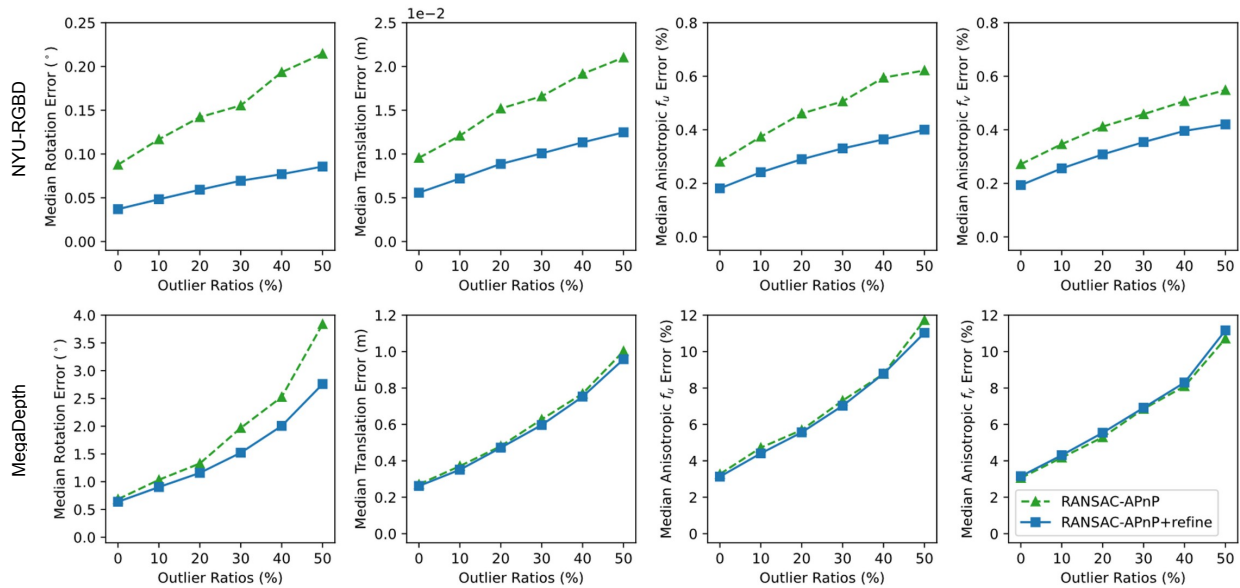


Figure 8. This is a supplementary figure to Fig. 7 in which we omit the comparisons with 6-point DLT.